Cryogenics 77 (2016) 36–42

Contents lists available at ScienceDirect

Cryogenics

journal homepage: www.elsevier.com/locate/cryogenics

Characterization of a thermoelectric/Joule–Thomson hybrid microcooler

H.S. Cao [a,*], S. Vanapalli [a], H.J. Holland [a], C.H. Vermeer [b], H.J.M. ter Brake [a]

[a] Energy, Materials and Systems, Faculty of Science and Technology, University of Twente, 7500 AE Enschede, The Netherlands
[b] SuperACT, Marterstraat 66, 7559 AJ Hengelo, The Netherlands

ARTICLE INFO

Article history:
Received 7 January 2016
Received in revised form 21 April 2016
Accepted 24 April 2016
Available online 29 April 2016

Keywords:
Joule–Thomson effect
Thermoelectric cooling
Microcooler
Cryogenic cooling

ABSTRACT

Micromachined Joule–Thomson (JT) coolers are attractive for cooling small electronic devices. However, microcoolers operated with pure gases, such as nitrogen gas require high pressures of about 9 MPa to achieve reasonable cooling powers. Such high pressures severely add complexity to the development of compressors. To overcome this disadvantage, we combined a JT microcooler with a thermoelectric (TE) pre-cooler to deliver an equivalent cooling power with a lower pressure or, alternatively, a higher cooling power when operating with the same pressure. This hybrid microcooler was operated with nitrogen gas as the working fluid at a low pressure of 0.6 MPa. The cooling power of the microcooler at 101 K operating with a fixed high pressure of 8.8 MPa increased from 21 to 60 mW when the precooling temperature was reduced by the thermoelectric cooler from 295 to 250 K. These tests were simulated using a dynamic numerical model and the accuracy of the model was verified through the comparison between experimental and simulation results. Based on the model, we found the high pressure of the microcooler can be reduced from 8.8 to 5.5 MPa by lowering the precooling temperature from 295 to 250 K. Moreover, the effect of TE cooler position on the performance of the hybrid microcooler was evaluated through simulation analysis.

1. Introduction

Many electronic devices can benefit from operation at lower temperatures, which results in lower thermal noise [1,2], higher speed [3], larger bandwidth [4], or even superconductivity [5,6]. Micromachined Joule–Thomson (JT) coolers are attractive for cooling these electronics, because they have no moving cold parts and, therefore, can be scaled down to match the size and power consumption of these electronics. JT microcoolers produce cooling power by the expansion of a high-pressure gas through a flow restriction. This cooling power can be increased by pre-cooling the incoming high-pressure gas by the cold low-pressure gas in a counter flow heat exchanger (CFHX). The temperatures of the low- and high-pressure gas flows will approach closest at some location, referred to as the pinch-point. The maximum possible cooling capacity per unit of mass flow is the minimum isothermal enthalpy difference (Δh_{min}) between the low- and high-pressure gas flows over the temperature range spanned by the CFHX. For pure gases, Δh_{min} usually occurs at the warm end of the heat exchanger. The isothermal enthalpy difference increases with increasing high pressure and with decreasing warm-end temperature. Usually, a high pressure is needed to achieve sufficient refrigeration, which adds complexity to the development of a compressor for the closed-cycle operation of a JT cooler.

In order to deliver an equivalent cooling power with modest high pressures, the high-pressure gas can be pre-cooled at the warm-end entrance of the CFHX. Precooling can be realized by using thermoelectric (TE) coolers. TE coolers are semiconductor devices that can directly convert electricity into cooling power at an interface [7]. TE coolers offer similar advantages as JT coolers, such as compact structure, free of moving parts, high reliability and spot cooling. Compared to TE coolers, JT coolers can reach lower temperatures with higher efficiencies [8–10]. Lester [11] investigated the possibility of increasing the efficiency of a closed cycle JT cooler by using a TE cooler. Precooling by a TE cooler at 240 K was employed in a closed cycle JT microcooling configuration by Burger et al. [12] and Lin et al. [13]. Burger et al. developed a 169 K microcooler with a cooling power of 200 mW when it was operated with ethylene gas between 0.2 and 1.5 MPa. Lin et al. realized a 140 K JT microcooler operating with a five-component mixture between 0.07 and 1.4 MPa. An open JT system for cooling an infrared detector array was investigated by Bailey [14]. The run time of the system was extended by using TE precooling. This paper describes a hybrid microcooler that combines a 100 K JT cooler with a TE cooler to increase the cooling power or reduce

* Corresponding author.
E-mail addresses: H.Cao@utwente.nl, HaishanCao@gmail.com (H.S. Cao).

http://dx.doi.org/10.1016/j.cryogenics.2016.04.012
0011-2275/

the high pressure of the JT cooler. In the next section, the performance improvement of a JT cooler through TE precooling is analyzed based on the assumption of ideal operation of CHFXs and pre-cooler. The measurement set-up is described in Section 3 and the simulation of the performance of the hybrid microcooler is explained in Section 4. Section 5 discusses the measurement and simulation of the performance of the hybrid microcooler. The paper is closed with conclusions in Section 6.

2. Analysis

The schematic of a JT microcooler with a pre-cooler and the corresponding thermodynamic cycles drawn in a temperature-entropy plot are shown in Fig. 1. The cooling capacity (gross cooling power of the hybrid microcooler) $\dot{Q}_{load}$ is defined by:

$$\dot{Q}_{load} = (h_6 - h_5)\dot{m} = \Delta h_{6,5}\dot{m} \tag{1}$$

Here, h is specific enthalpy, and $\dot{m}$ is the mass-flow rate.

If there is no heat flow from the environment to the CFHX and assuming the JT expansion to be isenthalpic, then $\Delta h_{6,5} = \Delta h_{7,3}$. Extending the energy balance to the total CFHX, we can write:

$$\Delta h_{6,5}\dot{m} = \Delta h_{8,1}\dot{m} + \dot{Q}_{pre} \tag{2}$$

where $\dot{Q}_{pre}$ is the precooling power.

To analyze the efficiency of this hybrid microcooler, its coefficient of performance (COP) in the steady state is derived. Furthermore, it is assumed that there are no parasitics and all cooling energy of the TE cooler is used for precooling the high-pressure gas of the JT microcooler. The COP of the hybrid microcooler is defined as the ratio of the gross cooling power of the JT microcooler and the sum of the electric power, W_{TE}, supplied to the TE cooler and the change in Gibbs free energy of the working fluid of the JT microcooler during compression, as follows:

$$\mathrm{COP} = \frac{\Delta h_{6,5}\dot{m}}{W_{TE} + (\Delta h_{1,8} - T_h \Delta s_{1,8})\dot{m}} \tag{3}$$

where T_h is the ambient temperature.

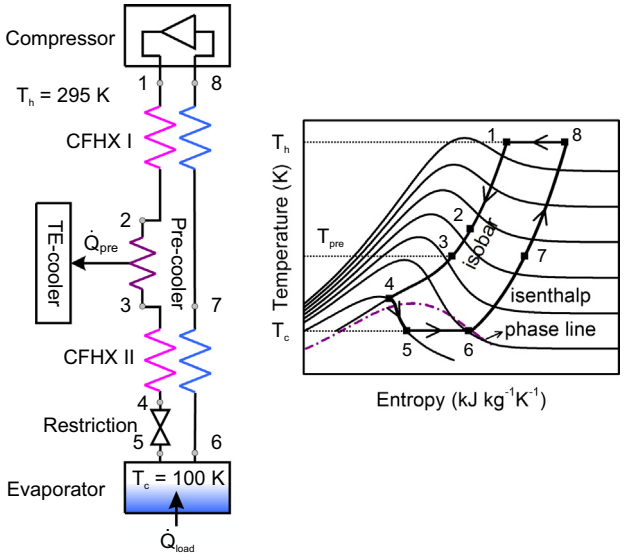

Fig. 1. A schematic of the Linde–Hampson cycle of a JT microcooler with a TE precooler and a temperature-entropy diagram representing the thermodynamic ideal cycles of the hybrid microcooler.

The COP of the TE cooler is defined as the ratio of the gross cooling power of the TE cooler, used as precooling power, $\dot{Q}_{pre}$, to the electric power input to the TE cooler:

$$\mathrm{COP}_{TE} = \frac{\dot{Q}_{pre}}{W_{TE}} \tag{4}$$

The steady-state energy balance of the pre-cooler gives:

$$\dot{Q}_{pre} = \Delta h_{2,3}\dot{m} \tag{5}$$

Substituting Eqs. (2), (4) and (5) into Eq. (3) results in:

$$\mathrm{COP} = \frac{\Delta h_{8,1} + \Delta h_{2,3}}{\Delta h_{2,3}/\mathrm{COP}_{TE} + (\Delta h_{8,1} - T_h \Delta s_{8,1})} \tag{6}$$

The overall COP of a multi-stage TE cooler, is a function of the COP of each stage. We consider an n-stage TE cooler with the COP of each stage to be equal and denoted by COP^*_{TE}. Then, the overall COP_{TE} is [15],

$$\mathrm{COP}_{TE} = \left((1 + 1/\mathrm{COP}^*_{TE})^n - 1\right)^{-1} \tag{7}$$

The COP of each stage of the n-stage TE cooler is given by an approximate expression [15]:

$$\mathrm{COP}^*_{TE} = n\left(\mathrm{COP}^S_{TE} + 0.5\right) - 0.5 \tag{8}$$

Here, it has been assumed that the temperature of each stage is equal to $(T^h_{TE} - T^c_{TE})/n$, where T^c_{TE} and T^h_{TE} are the cold- and warm-side temperatures of the TE cooler. Then COP^S_{TE} is given by [15,16]:

$$\mathrm{COP}^S_{TE} = \frac{T^c_{TE}\left((1+ZT)^{0.5} - T^h_{TE}/T^c_{TE}\right)}{\left(T^h_{TE} - T^c_{TE}\right)\left((1+ZT)^{0.5} + 1\right)} \tag{9}$$

where $ZT = S^2\sigma/\kappa$ is the figure-of-merit of the TE cooler, S, σ, κ and T are the Seebeck coefficient, the electrical conductivity, the thermal conductivity and the absolute temperature, respectively [17].

The hybrid microcooler discussed in this paper uses a two-stage TE cooler. Therefore, the COP of a two-stage TE cooler will be analyzed. Fig. 2a shows the COP of a two-stage TE cooler with the warm side at 295 K as a function of the cold-side temperature for several figures-of-merit. The COP increases with an increasing figure-of-merit at a fixed cold-side temperature and approaches the Carnot-cycle efficiency for an infinite ZT. The efficiency of the TE cooler for a constant figure-of-merit rapidly decreases with increasing temperature difference between the warm and cold side.

The relation between the COP of the hybrid microcooler and the precooling temperature is shown in Fig. 2b. The working fluid of the JT microcooler is nitrogen gas, and the high and low pressures of the nitrogen gas are 8.8 and 0.6 MPa, respectively. The COP of the hybrid microcooler increases with increasing figure-of-merit of the TE-cooler for a constant precooling temperature. At a constant figure-of-merit a lower precooling temperature is beneficial but at too low temperatures the COP decreases due to the decreasing COP of the TE cooler. Commercially available TE materials [16] have a figure-of-merit, ZT, of about 1. According to Fig. 2b the optimal precooling temperature with ZT equal to 1 is about 230 K and the corresponding COP is about 0.1.

Fig. 3a shows the gross cooling power of the hybrid microcooler per unit of mass-flow rate of nitrogen gas (kg s^{-1}) as a function of the precooling temperature for several high pressures. Here, the low pressure of the JT microcooler is set to a constant value of 0.6 MPa. This specific gross cooling power of the hybrid microcooler increases with increasing high pressure and decreasing precooling temperature. The specific gross cooling power of the hybrid

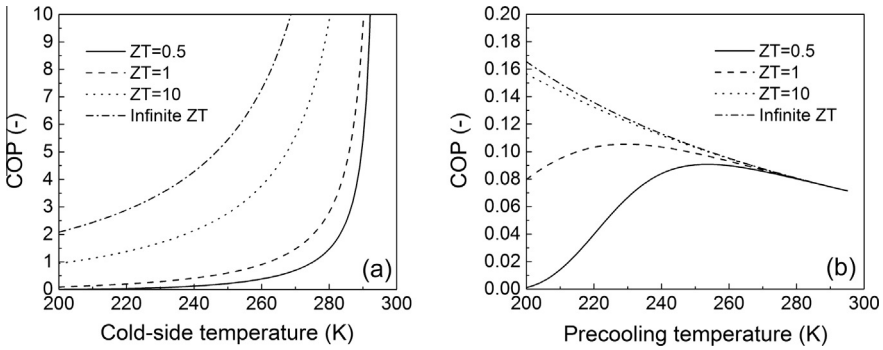

Fig. 2. (a): COP of a two-stage TE cooler as a function of cold-side temperature for different figures-of-merit, *ZT*; (b): COP of the hybrid microcooler with TE precooling as a function of the precooling temperature for different *ZT* values. The warm-side temperature of the TE cooler is 295 K. The working fluid of the JT microcooler is nitrogen gas between 0.6 and 8.8 MPa.

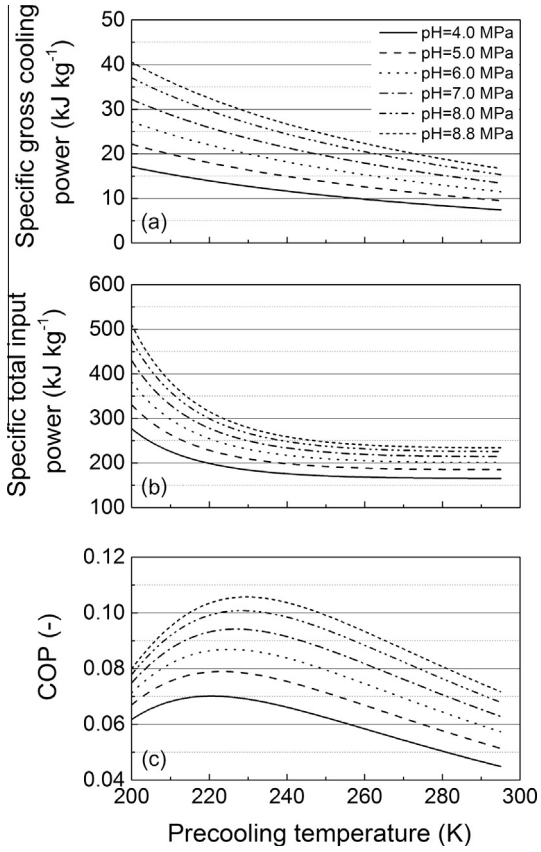

Fig. 3. Specific gross cooling power (a), specific total input power (b) and COP (c) of the hybrid microcooler with a two-stage TE precooler as a function of precooling temperature for different high pressures. The figure-of-merit, *ZT*, of the material of the TE cooler is 1 and the warm-side temperature of the TE cooler is 295 K. The low pressure of the JT microcooler is 0.6 MPa.

microcooler without precooling at a high pressure of 8.8 MPa is about the same as that of the hybrid microcooler precooled to a temperature of 250 K with a high pressure of 6.0 MPa. Hence, the precooling in a hybrid microcooler relaxes the requirement of high pressure for reaching the same cooling power.

Fig. 3b shows the total specific input power of the hybrid microcooler (sum of the ideal compressor power and the electric power supplied to TE cooler power) as a function of the precooling temperature for several high pressures. The total input power of the hybrid microcooler at a constant precooling temperature increases with increasing high pressure of the nitrogen gas. At a constant high pressure, the precooling temperature has little influence on the total input power of the hybrid microcooler when the precooling temperature is higher than 240 K. That is because the input power of the TE cooler power is much smaller than the compressor power, which is independent of the precooling temperature. However, when the precooling temperature is reduced to below 240 K, the COP of the TE cooler power gets very low, which causes the total input power of the hybrid microcooler to increase rapidly with decreasing precooling temperature.

Fig. 3c shows the resulting COP of the hybrid microcooler as a function of the precooling temperature for several high pressures. It increases with increasing high pressure of the nitrogen gas. At a fixed high pressure, the COP of the hybrid microcooler shows a maximum that for all cases is around 230 K. This maximum is determined by the performance of the TE cooler as shown in Fig. 2b. In this analysis, the hybrid microcooler without precooling at a high pressure of 8.8 MPa has almost the same COP as that of the hybrid microcooler precooled to a temperature of 250 K with a high pressure of only 5.0 MPa.

3. Measurement setup

In the experimental set-up, the working fluid, nitrogen gas (purity level 5.0) is supplied from a pressurized gas bottle. The gas flows through a pressure controller and a getter filter to the microcooler. The getter filter is used to remove impurities from the gas (especially water) to about 1.0 part per billion (ppb) level to prevent clogging due to water deposition [18]. The microcooler is mounted in a glass vacuum chamber where a pressure of less than 0.01 Pa is maintained. At the low-pressure side, the pressure of the gas is measured with a pressure meter, and the outflow is measured with a mass-flow meter. A pressure relief valve is used at the outlet to maintain a constant outlet pressure and also to prevent air from flowing into the system.

The hybrid microcooler used in the experiments and its cross section are shown in Fig. 4a–c. The JT microcooler made of borosilicate glass (D263T) has outer dimensions of 60.0 mm × 9.5 mm × 0.72 mm. The height of the gas channels in the CFHX is 40 μm. The JT restriction consists of 7 parallel rectangular slits with a length of 2.8 mm, a width of 0.14 mm and a height of 1.1 μm. With respect to the microcooler, the cold interface of the TE cooler has a width of 8.8 mm and a length of 6.6 mm. The center of the TE cooler is located at a distance of 28 mm from the cold end of the JT microcooler. The length and width of the silicon piece between the JT microcooler and the cold side of the TE cooler both are 9.5 mm. The hybrid microcooler is mounted into a flange and surrounded by a printed circuit board (PCB) as shown in Fig. 4d. A heat sink made of braided copper wire is used to transfer the heat that is

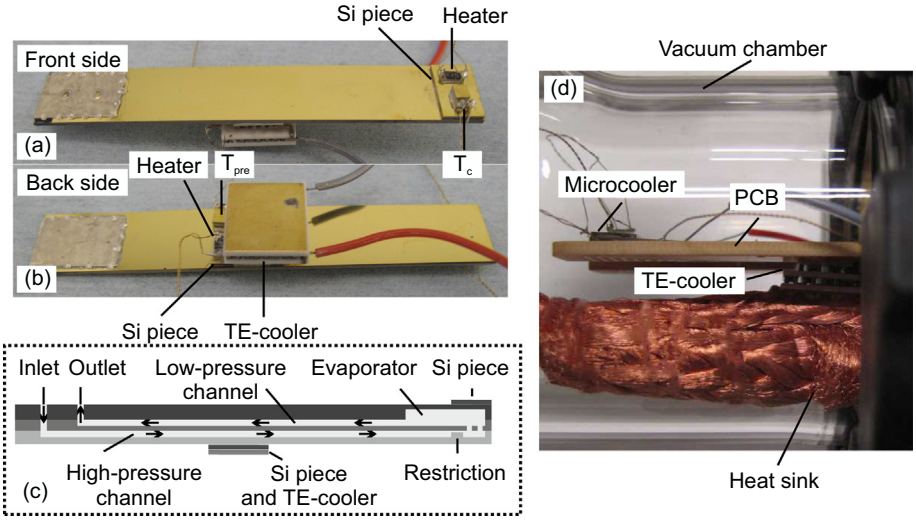

Fig. 4. Top side (a) and back side (b) of the JT microcooler with a two-stage TE cooler, two silicon pieces, two heaters and two temperature sensors. (c) Schematic cross-section of the hybrid microcooler. (d) Hybrid microcooler mounted into a vacuum chamber and surrounded by a PCB.

rejected by the TE cooler to the outside of the vacuum chamber. The temperatures are measured with DT diode sensors at the cold end of the microcooler and at the pre-cooler indicated by T_c and T_{pre}, respectively (temperature sensor locations shown in Fig. 4a and b). Surface-mounted-device resistors are used as heaters for supplying heat in order to control the temperature and measure the cooling power. The function of the silicon pieces is to uniformly distribute the heat generated by the heaters or the cooling produced by the TE cooler. The temperature sensors, heaters and silicon pieces are glued on the microcooler with silver paint and connected to the PCB using manganin wires with a diameter of 100 μm. The gas inlet and outlet ports of the microcooler are connected to the tubes with indium seals for leak tightness.

4. Modelling

In order to simulate the performance of the hybrid microcooler, a dynamic numerical model was developed. In the model, the hybrid microcooler is divided into four parts (two CFHXs, an evaporator and a pre-cooler) as shown in Fig. 5. These parts are connected by enthalpy flow ($\dot{H}$) and longitudinal conductive heat flow ($\dot{Q}_c$). In addition, the radiative heat flow ($\dot{Q}_{rad}$) on the microcooler outer surface and conductive heat flow via the surrounding gas ($\dot{Q}_{csg}$) are taken into account. The CFHXs and the pre-cooler are split into elements of constant length and each element contains three sub-elements: a high-pressure fluid element, a material element and a low-pressure fluid element. The evaporator is treated as a single element. In the CFHX elements again enthalpy flow, conductive heat flow and radiation play a role, but also convective heat exchange between wall and fluid is taken into account. In the simulation, we assume that material elements of the pre-cooler have the same temperature as that of the silicon piece between the JT microcooler and the TE cooler (see Fig. 4). A more detailed discussion on the modelling of the CFHXs can be found in an earlier study [19].

5. Measurement and simulation results

5.1. Effect of precooling temperature

The JT microcooler was operated with nitrogen gas at a high pressure of 8.8 MPa and a low pressure of 0.6 MPa. At a precooling temperature (T_{pre}) of 250 K, the cold-end temperature (T_c) of the JT microcooler decreased from 295 to 99 K in about 20 min (see Fig. 6). The mass-flow rate increased from 0.67 to 4.1 mg s^{-1} and fluctuated at around 3.2 mg s^{-1} after 20 min. The cooling power available at several precooling temperatures was measured by controlling T_c at 101 K with a heater at the cold end of the microcooler in a PID control loop. As shown in Fig. 6, the mass-flow rate of the microcooler increased gradually from 3.2 to 3.6 mg s^{-1} with the cold-end temperature increasing from 99 to 101 K. With T_c controlled at 101 K, no excess liquid nitrogen will be present in the return line anymore. As a result the temperature profile along the restriction changed and since the flow rate depends on fluid density and viscosity (both temperature dependent), also the

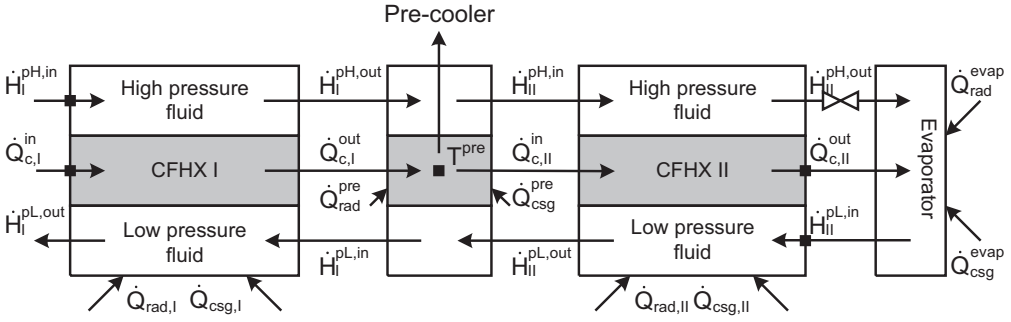

Fig. 5. Block diagram of the dynamic model of the hybrid microcooler. Temperature nodes indicated by rectangular symbol serve as boundary conditions.

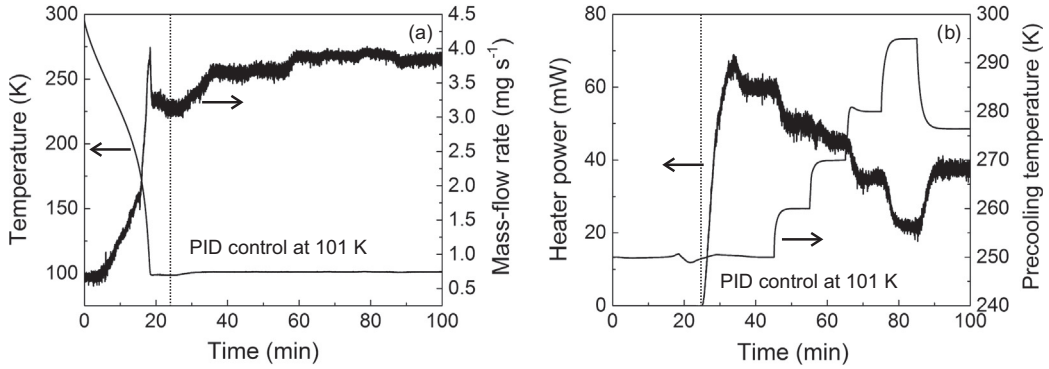

Fig. 6. Measurement results of the hybrid microcooler operated with a high pressure of 8.8 MPa, a low pressure of 0.6 MPa and several precooling temperatures. (a) Cold-end temperature (T_c) and mass-flow rate of the microcooler versus time. (b) Cooling power of the microcooler and the precooling temperature (T_{pre}) of the TE cooler versus time.

mass-flow rate changed. The heater power required for stabilizing T_c at 101 K (indicating the net cooling power at that temperature) was about 60 mW with a mass-flow rate of 3.65 mg s^{-1}. The method is repeated to measure the net cooling power at several precooling temperatures (see Fig. 6).

The net cooling power of the microcooler at different precooling temperatures was calculated using the model discussed in Section 3 and the measured mass-flow rate and temperature as inputs. The measured and calculated results are summarized in Table 1. The difference between the measured and the calculated net cooling power is within 7 mW. The calculated precooling power indicates the heat absorbed by the TE cooler from the JT microcooler, which decreased with increasing precooling temperature. In case '*f*' shown in Table 1, the TE cooler was switched off and the precooling temperature was not controlled during the measurement. The calculated precooling power in this case was −7 mW, which can be due to the conduction between the heat sink and the microcooler. At even higher temperature, the TE element had to apply heat instead of cooling in order to stabilize at the set-point 'precooling' temperature.

5.2. Effect of high pressure

Fig. 7 shows the cooling power of the hybrid microcooler at 101 K with a constant precooling temperature of 250 K. The JT microcooler was operated at a constant low pressure of 0.6 MPa and several high pressures. As the high pressure decreased from 8.8 to 6.0 MPa, the mass-flow rate decreased from 3.65 to 3.24 mg s^{-1}, and the corresponding net cooling power decreased from 60 to 2 mW. The unstable heat powers in the cases of 8.0 and 7.0 MPa were caused by the reducing mass-flow rates due to water depositing in the JT restriction [18]. To reduce the deposition rate, three measures are proposed. The first measure is to decrease the water fraction in the supply gas using a filter at cryogenic temperatures rather than at room temperature. The second measure is to the increase the length of the silicon piece glued on the cold end of the JT microcoler to make a thermal link between evaporator and the relevant part of the CFHX [18]. The third measure is to replace the designed restriction with a height-to-width ratio of 1.1/140 by a longer restriction with a larger height-to-width ratio.

The measurement details are listed in Table 2, which also includes the calculated cooling power based on the measured mass-flow rates and temperatures. The maximum difference between the measured and the predicted net cooling power was about 2 mW in the considered measuring range as shown in Table 2. The calculated precooling power that was required to stabilize at 250 K decreased with reducing high pressure and mass-flow rate.

Comparison of Figs. 6 and 7 indicates that the cooling power of the microcooler operating at a high pressure of 8.8 MPa and a precooling temperature of 295 K is almost equal to that of the microcooler operating at a high pressure of 7.0 MPa and a precooling temperature of 250 K, which is about 20 mW. However, the mass-flow rates, the efficiencies of the CFHX of the two cases are different, respectively. Assume, by redesigning the cooler, we can realize a mass-flow rate of 3.9 mg s^{-1} at a precooling temperature of 250 K. Then, our model indicates that a pressure of only 5.5 MPa would be required to establish a cooling power of 20 mW.

5.3. Effect of TE cooler position

The effect of the TE cooler position on the performance of the hybrid microcooler was evaluated using the above-discussed model of which the accuracy was validated by the comparison between experimental and simulation results. In the measurement set-up, the center of the TE cooler is located at a distance of 28 mm from the cold end of the JT microcooler. The position of the TE cooler determines the lengths of CFHXs I and II of the JT microcooler under test, which in turn determine the efficiencies of these CFHXs. In the simulation analysis, the hybrid microcooler was assumed to be operated with a high pressure of 8.8 MPa, a low pressure of 0.6 MPa and a precooling temperature of 250 K. As shown in Fig. 8, the net cooling power of the microcooler increases as the TE cooler is shifted from the cold end to the warm end of the JT microcooler because of the higher efficiency of CFHX II. And meanwhile, the required precooling power also increases due to

Table 1
Cooling power of the hybrid microcooler at 101 K and precooling power of the TE cooler at several precooling temperatures. The JT microcooler was operated between 8.8 and 0.6 MPa.

Case	*a*	*b*	*c*	*d*	*e*	*f*
Measured precooling temp. (K)	250	260	270	280	295	276
Measured mass-flow rate (mg s^{-1})	3.65	3.67	3.87	3.90	3.92	3.90
Measured cooling power (mW)	60	50	44	35	21	38
Calculated cooling power (mW)	58	47	40	29	14	34
Calculated precooling power (mW)	37	19	2	−15	−41	−7

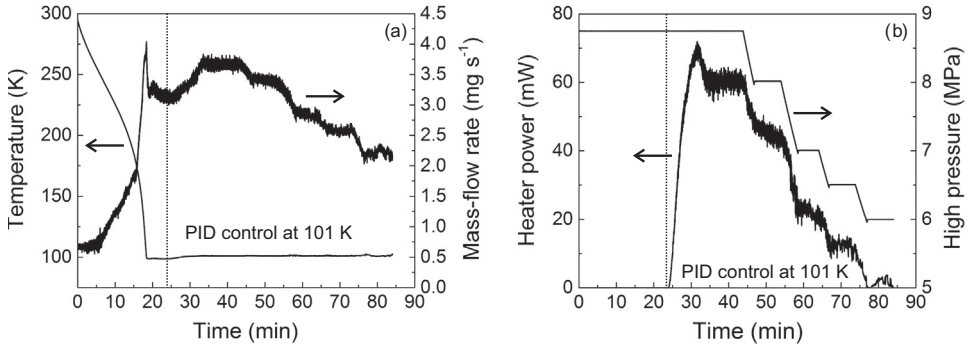

Fig. 7. Measurement results of the hybrid microcooler operated with a low pressure of 0.6 MPa, a precooling temperature of 250 K and several high pressures. (a) Cold-end temperature (T_c) and mass-flow rate of the microcooler versus time. (b) Cooling power and high pressure of the microcooler versus time.

Table 2
Cooling power of the microcooler at 101 K and precooling power of the TE cooler at different high-pressure settings. The microcooler was operated with a low pressure of 0.6 MPa and a precooling set-point temperature of 250 K.

Case	*a*	*b*	*c*	*d*	*e*
Measured high pressure (MPa)	8.8	8.0	7.0	6.5	6.0
Measured mass-flow rate (mg s^{-1})	3.65	3.42	2.88	2.56	2.24
Measured cooling power (mW)	60	45	23	12	2
Calculated cooling power (mW)	58	44	22	10	0
Calculated precooling power (mW)	37	31	23	18	15

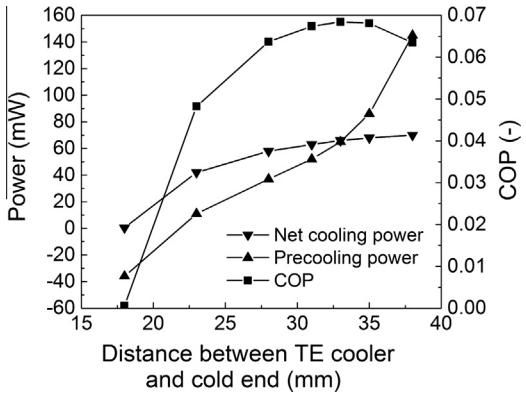

Fig. 8. Effect of the TE cooler position on the performance of the hybrid microcooler operated with a high pressure of 8.8 MPa, a low pressure of 0.6 MPa and a precooling temperature of 250 K.

the decreasing efficiency of CFHX I. When the distance between the center of the TE cooler and the cold end is 18 mm, the precooling power is −36 mW, which means the TE cooler applies heat instead of cooling. As the distance increases to 33 mm, the COP of the hybrid microcooler reaches the peak value of 0.068. Further increase in the distance has little effect on the efficiency of CFHX II and none on the net cooling power. However, the required precooling power increases greatly, caused by the decreasing efficiency of CFHX I due to the lower length of CFHX I.

6. Conclusions

A hybrid microcooler consisting of a JT microcooler and a TE cooler has been developed and tested. The effects of the precooling temperature of the TE cooler, the operating high pressure of the JT microcooler and the position of the TE cooler on the cooling power of the hybrid microcooler were investigated. The JT microcooler was operated with nitrogen gas at a low pressure of 0.6 MPa. With a fixed high pressure of 8.8 MPa, the cooling power of the hybrid microcooler at 101 K increased from 21 to 60 mW when the precooling temperature was reduced by the thermoelectric element from 295 to 250 K. A dynamic numerical model was developed for simulating the performance of the hybrid microcooler and this model was validated with the experimental results. Based on the model, we found that the high pressure of the microcooler can be reduced from 8.8 to 5.5 MPa by lowering the precooling temperature from 295 to 250 K. In general, we can conclude that the integration of a JT microcooler with a TE cooler relaxes the requirements of the compressor and/or may be used to increase the cooling performance.

Acknowledgments

This work is supported by NanoNextNL, a micro and nanotechnology consortium of the Government of the Netherlands and 130 partners.

References

[1] Rogalski A. Infrared detectors: status and trends. Prog Quant Electron 2003;27(2-3):59–210. http://dx.doi.org/10.1016/S0079-6727(02)00024-1.
[2] Kessler T, Hagemann C, Grebing C, Legero T, Sterr U, Riehle F, et al. A sub-40-MHz-linewidth laser based on a silicon single-crystal optical cavity. Nature Photon 2012;6(10):687–92. http://dx.doi.org/10.1038/NPHOTON.2012.217.
[3] Laskar J, Maranowski S, Kruse J, Ketterson A, Adesida I, Feng M, et al. High speed cryogenic operation of sub-micron pseudomorphic ingaas/gaas fets. In: Proceedings IEEE/cornell conference on advanced concepts in high speed semiconductor devices and circuits. p. 445–54. http://dx.doi.org/10.1109/CORNEL.1991.170014.
[4] Wadefalk N, Mellberg A, Angelov I, Barsky ME, Bui S, Choumas E, et al. Cryogenic wide-band ultra-low-noise if amplifiers operating at ultra-low dc power. IEEE Trans Microwave Theory Tech 2003;51(6):1705–11. http://dx.doi.org/10.1109/TMTT.2003.812570.
[5] Clarke J. Squids for everything. Nature Mater 2011;10(4):262–3. http://dx.doi.org/10.1038/nmat2996.
[6] Nisenoff M. Cryocoolers and high-temperature superconductors: advancing toward commercial applications. In: Ross RG, editor. Cryocoolers, vol. 8. p. 913–7. http://dx.doi.org/10.1007/978-1-4757-9888-3_89.
[7] Sales BC. Thermoelectric materials – smaller is cooler. Science 2002;295(5558):1248–9. http://dx.doi.org/10.1126/science.1069895.
[8] Gong M, Sun Z, Wu J, Zhang Y, Meng C, Zhou Y. Performance of R170 mixtures as refrigerants for refrigeration at −80 °C temperature range. Int J Refrig – Revue Int Du Froid 2009;32(5):892–900. http://dx.doi.org/10.1016/j.ijrefrig.2008.11.007.
[9] Narasimhan NL, Venkatarathnam G. Studies on the performance of a small reciprocating compressor with different nitrogen hydrocarbon mixtures. Int J Refrig – Revue Int Du Froid 2013;36(8):2091–6. http://dx.doi.org/10.1016/j.ijrefrig.2013.07.011.
[10] Damle RM, Atrey MD. Transient simulation of a miniature Joule–Thomson (J–T) cryocooler with and without the distributed J–T effect. Cryogenics 2015;65:49–58. http://dx.doi.org/10.1016/j.cryogenics.2014.10.003.
[11] Lester J. Closed cycle hybrid cryocooler combining the Joule–Thomson cycle with thermoelectric coolers. In: Fast RW, editor. Advances in cryogenic

engineering, Proceedings of the 1989 cryogenic engineering conference, vol. 35B; 1990. p. 1335–40.
[12] Burger JF, Holland HJ, Seppenwoolde JH, Berenschot E, ter Brake HJM, Gardeniers JGE, et al. 165 K microcooler operating with a sorption compressor and a micromachined cold stage. In: Ross RG, editor. Cryocoolers, vol. 11. p. 551–60. http://dx.doi.org/10.1007/0-306-47112-4_69.
[13] Lin MH, Bradley PE, Huber ML, Lewis R, Radebaugh R, Lee YC. Mixed refrigerants for a glass capillary micro cryogenic cooler. Cryogenics 2010;50 (8):439–42. http://dx.doi.org/10.1016/j.cryogenics.2010.04.004.
[14] Bailey TB. Hybrid thermoelectric/Joule–Thomson cryostat for cooling detectors. US Patent 5,551,244; September 3 1996. <http://www.google.com/patents/US5551244>.
[15] Prasad M. Refrigeration and air conditioning. New Delhi: New Age International (P) Ltd.; 2003.
[16] Yang B, Ahuja H, Tran TN. Thermoelectric technology assessment: application to air conditioning and refrigeration. HVAC&R Res 2008;14(5):635–53. http://dx.doi.org/10.1080/10789669.2008.10391031.
[17] Bell LE. Cooling, heating, generating power, and recovering waste heat with thermoelectric systems. Science 2008;321(5895):1457–61. http://dx.doi.org/10.1126/science.1158899.
[18] Cao HS, Vanapalli S, Holland HJ, Vermeer CH, ter Brake HJM. Clogging in micromachined Joule–Thomson coolers: mechanism and preventive measures. Appl Phys Lett 103(3). doi:http://dx.doi.org/10.1063/1.4815987.
[19] Cao H, Mudaliar A, Derking J, Lerou P, Holland H, Zalewski D, et al. Design and optimization of a two-stage 28 K Joule–Thomson microcooler. Cryogenics 2012;52(1):51–7. http://dx.doi.org/10.1016/j.cryogenics.2011.11.003.